Journal of Alloys and Compounds 509 (2011) 8365–8369

Contents lists available at ScienceDirect

Journal of Alloys and Compounds

journal homepage: www.elsevier.com/locate/jallcom

Growth and optical spectroscopy of KPb_2Cl_5 crystal containing Mn^{2+}

Guohua Jia, Huanping Wang, Cuifang Wang, Shilong Zhao, Degang Deng, Lihui Huang, Youjie Hua, Chenxia Li, Shiqing Xu*

College of Materials Science and Engineering, China Jiliang University, Hangzhou 310018, PR China

ARTICLE INFO

Article history:
Received 25 March 2011
Received in revised form 1 May 2011
Accepted 4 May 2011
Available online 2 June 2011

Keywords:
Crystal growth
KPb_2Cl_5
Mn^{2+} spectroscopy
Tanabe–Sugano diagram

ABSTRACT

KPb_2Cl_5:Mn^{2+} crystal with sizes of centimeters has been successfully grown by a modified Bridgman method. The electronic spectra of Mn^{2+} in the title compound have been measured at different temperatures and compared, revealing that the red emission observed at 10 and 77 K in the spectral range from 500 to 800 nm, which vanishes at room temperature, is associated with the radiation from Pb^{2+} ions with adjacent defects whereas the orange-red emission in the spectral range from 530 to 680 nm can be undoubtedly attributed to the spin forbidden transition $^4T_{1g}$ (^4G) → $^6A_{1g}$(^6S) of Mn^{2+}. The electronic excitation spectra are interpreted in a strong crystal field scheme with the use of the Tanabe–Sugano diagram. Good agreement with the experimental spectroscopic data is obtained with the use of crystal field splitting parameter $10Dq = 7902\ cm^{-1}$, Racah parameters $B = 618\ cm^{-1}$, and $C = 3549\ cm^{-1}$.

1. Introduction

Potassium lead chloride (KPb_2Cl_5) is one of the few non-hygroscopic chloride hosts which can be easily handed within air and have good chemical and mechanical stabilities. According to the Raman scattering spectra, the maximum phonon energy of the KPb_2Cl_5 lattice is only ~202 cm^{-1} so that the multiphonon relaxation rates are low [1]. This crystal has a broad transparency in the spectral range from 0.3 to 22 μm [2]. The above favorable properties of KPb_2Cl_5 enable it to serve as an attractive material for upconversion, infrared lasing, and anti-Stokes cooling [3–10].

KPb_2Cl_5 crystallizes into the monoclinic system with $P2_1/c$ (14) space group, with $a = 8.854(2)$, $b = 7.927(2)$, $c = 12.485(3)$, $\beta = 90.05(3)^\circ$, $V = 876.3(4)\ Å^3$, $Z = 4$, and $d = 4.78(1)\ g\ cm^{-3}$ [11]. The X-ray single crystal diffraction analysis of KPb_2Cl_5 shows that there are two distinct Pb^{2+} sites, Pb(1) and Pb(2), each having a C_1 site symmetry. Pb(1) and Pb(2) coordinate with six and seven chloride atoms, respectively (Fig. 1b). The ionic radii of high spin Mn^{2+} in VI and VII coordinations differ from those of six-fold coordinated Pb(1) and seven-fold coordinated Pb(2) by 30.3% and 26.8%, respectively [12], so that Mn^{2+} is expected to occupy predominantly both of the Pb(1) and Pb(2) sites without charge compensation. Although there is the possibility that Mn^{2+} accommodates on both of the above two non-equivalent sites, the electron paramagnetic resonance (EPR) spectroscopy reveals [13] that Mn^{2+} occupies one of the two distinct sites. In other cases of Er^{3+} doped KPb_2Cl_5, parallel works performed by Jenkins et al. [8], Gruber et al. [14], and Ferrier et al. [2] confirm that Er^{3+} ions accommodate on the Pb(2) site with a vacancy in the nearby K^+ site since the number of Stark levels is in good agreement with that of one distinct site rather than two. Therefore, in the following optical spectroscopic interpretation we will assume that Mn^{2+} entered one of the two distinct sites and the crystal field analysis will be performed based on this assumption. With some approximation, one can roughly assume that Mn–Cl polyhedra in Mn^{2+} doped KPb_2Cl_5 form a distorted $MnCl_6^{4-}$ octahedron since tetrahedra only present when Mn^{2+} coordinates with less chloride atoms, e.g. $MnCl_4^{2-}$. The unit cell of KPb_2Cl_5 and the nearest-neighbor coordination environments of Pb(1) and Pb(2) are shown in Fig. 1a and b, respectively.

The optical spectroscopy and the demonstration of lasing of KPb_2Cl_5 doped with rare earth ions have been extensively studied [3–18]. However, to the best of our knowledge, there are rare reports on the growth and optical spectroscopy of transition metal doped KPb_2Cl_5. Neamtu and Darabont [13] have reported the melt growth of KPb_2Cl_5 crystal containing Mn^{2+} and concluded that Mn^{2+} ions only accommodate on one (with low site symmetry) of the two distinct Pb^{2+} site based on the electron paramagnetic resonance (EPR) measurement. However, they did not provide any EPR spectrum and the above conclusion is not consist with any structural analysis since both Pb(1) and Pb(2) have the same C_1 site symmetry from previous structural analysis [11]. The optical spectroscopy of Mn^{2+} has not ever been investigated and interpreted yet. There are several reports on the crystal growth of KPb_2Cl_5 by the Bridgman method [13,19–23]. However, it still remains a challenge to grow KPb_2Cl_5 crystal into centimeter sizes with good optical quality since there are many difficulties associated with

* Corresponding author.
E-mail addresses: ghjia@hotmail.com (G. Jia), sxucjlu@hotmail.com (S. Xu).

0925-8388/$ – see front matter © 2011 Elsevier B.V. All rights reserved.
doi:10.1016/j.jallcom.2011.05.010

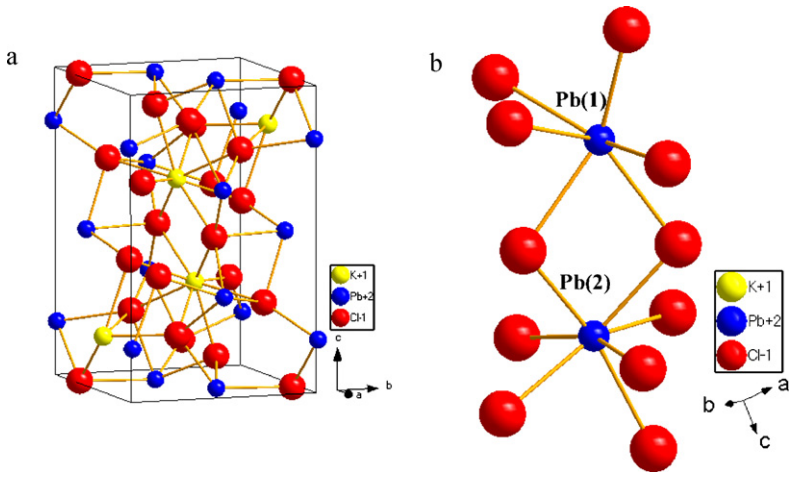

Fig. 1. (a) Unit cell of KPb_2Cl_5 and (b) local coordination geometry environment of Pb(1) and Pb(2).

different steps of the growth process [20,21]. The incorporation of oxide impurities, the reproducible seeding, and cracking induced by the phase transition prevent KPb_2Cl_5 from growing into bulk crystals with high quality and those problems should be solved before it find application in lasing.

Herein, bulk KPb_2Cl_5 containing Mn^{2+} with sizes of centimeters and good optical quality has been grown by a modified Bridgman method. The optical spectroscopy of Mn^{2+} in KPb_2Cl_5 at different temperatures has been measured, compared and interpreted with the use of the Tanabe–Sugano diagram [24]. The crystal field splitting parameter $\Delta E = 10Dq$ and the Racah parameters B and C of Mn^{2+} in the title compound have been obtained and compared with those in other types of hosts. The room temperature lifetime of $^4T_{1g}(^4G)$ of Mn^{2+} obtained by different excitation wavelengths has been measured and compared.

2. Experimental

2.1. Preparation

Bulk KPb_2Cl_5 crystal was grown by a modified Bridgman method as previous described in Ref. [23]. Chemicals were used as received without further purification. Stoichiometric amounts of KCl (99.9%, Aldrich) and $PbCl_2$ (99.9%, Aldrich) containing 0.5 at.% $MnCl_2$ (99.999%, Aldrich) powders were heated in a furnace filled with argon at 300 °C for 6 h to remove the residual water in the starting materials. The starting materials were thoroughly mixed and pressed into a quartz tube. The quartz tube was sealed under the vacuum of 10^{-3} Pa and then transferred into a vertical Bridgman furnace. The furnace was heated to 480 °C for a week. The bulk crystal was cut into pieces and then were polished afterwards. The as-grown crystal and polished species were shown in Fig. 2a and b, respectively. The polished species are transparent without cracking.

2.2. Characterization

X-ray powder diffraction (XRD) pattern was obtained by a CAD4 diffractometer using Cu Kα radiation (λ = 1.54056 Å) with a scanning rate of 1.5° min^{-1} in the angle range from 5° to 70°. The emission and excitation spectra were measured by a Horiba Jobin Yvon Fluorolog spectrofluorometer using a xenon-lamp as the light source and a TBX-04-A single-photon detection module. For lifetime measurements, the emission was analyzed with a 0.25 m Jobin-Yvon monochromator and the signal detected by a Hamamatsu R636 photomultiplier. For low temperature measurements, all samples were mounted on a closed cycle cryostat (10–350 K, DE202, Advanced Research Systems).

3. Results and discussion

3.1. XRD

The XRD pattern of KPb_2Cl_5:0.05%Mn^{2+} sample together with the standard pattern as the reference is shown in Fig. 3. Although the XRD pattern of KPb_2Cl_5 powder in our work looks a little bit noisy, no extra peaks are observed. The peaks in the powder sample

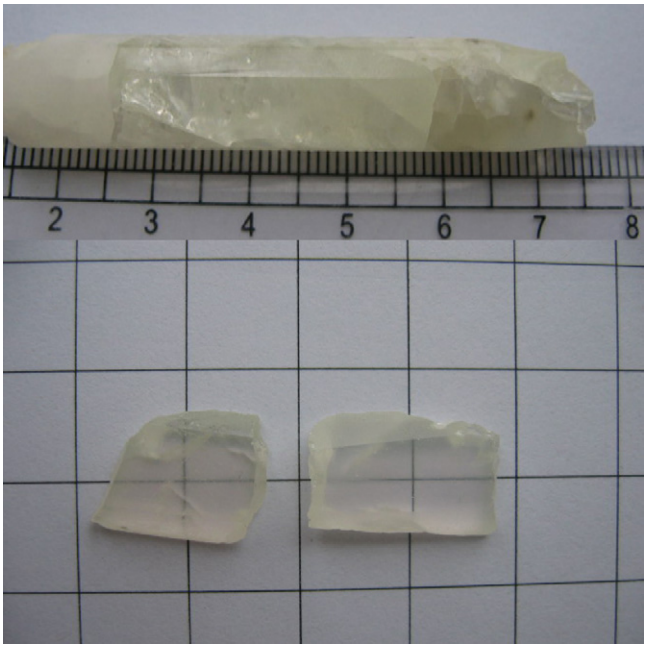

Fig. 2. The as-grown crystal and the polished species cut from the bulk crystal.

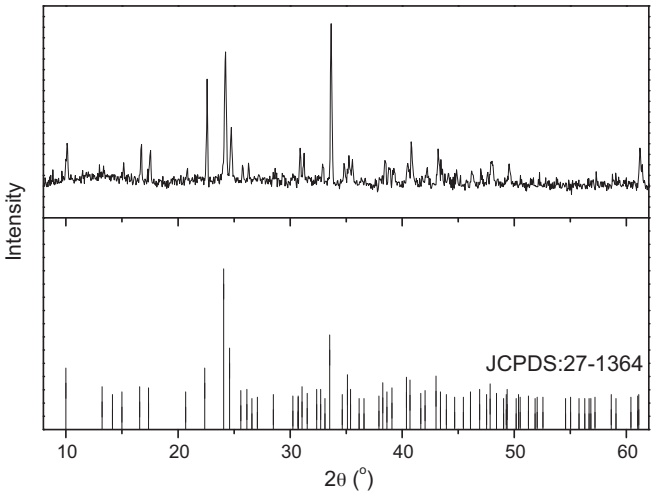

Fig. 3. XRD pattern of KPb_2Cl_5:0.5% Mn^{2+} powder sample. The standard data of KPb_2Cl_5 (JCPDS: 27-1364) is given for reference.

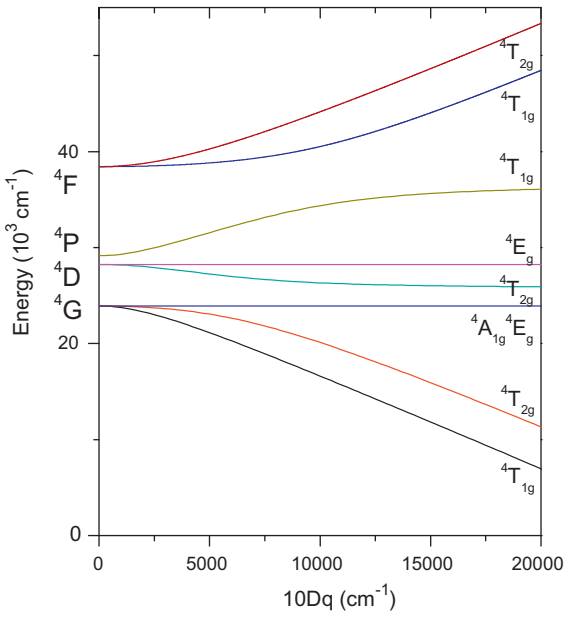

Fig. 4. Splitting of Mn^{2+} in an octahedral crystal field computed for $B = 618\ cm^{-1}$ and $C = 3549\ cm^{-1}$.

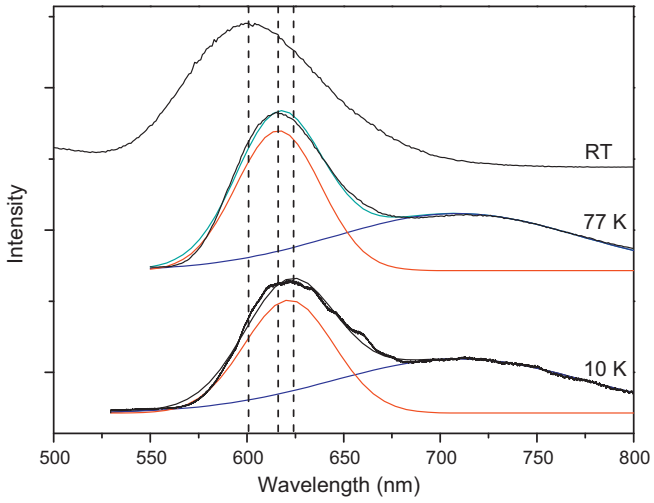

Fig. 6. Survey 10 K, 77 K and room temperature emission spectra of Mn^{2+} in KPb_2Cl_5 excited by 355 nm.

are in good agreement with those in the standard pattern (JCPDS: 27-1364).

3.2. Optical spectroscopy of Mn^{2+} in KPb_2Cl_5

The electronic absorption, excitation and emission spectra of Mn^{2+} have been extensively investigated in a wide variety of hosts [25–34]. As far as the emission color of Mn^{2+} activated phosphors is concerned, it falls into two classes: those with green emission and those with green-to-red emission [35,36]. The energy of the emission associated with the transition from $^4T_{1g}(^4G)$ to the ground state $^6A_{1g}(^6S)$ is strongly depended on the crystal splitting parameter $\Delta E = 10Dq$, as shown in the Tanabe–Sugano diagram in Fig. 4. In the case of Mn^{2+} incorporated into KPb_2Cl_5 crystal, the coordination environment of Mn^{2+} has been discussed in Section 1 and Mn^{2+} ions have been assumed to accommodate on the Pb site, which form a distort octahedron. The ground state of Mn^{2+} with the octahedral coordination is $^6A_{1g}$ and all optical electronic transitions are associated with the transition from the quartet ^4L (L = G, D, P, and F) to the sextet $^6A_{1g}$, which are both parity and spin forbidden. The microscopic origin of the sharp bands associated with the spin forbidden transition was recently discussed by Trueba et al. [37]. Therefore the spectra are very sharp and the molar absorption coefficient is two orders of magnitudes lower than for those parity and spin allowed transitions of other transition metal, e.g. Cr^{3+}.

The 77 K emission and excitation spectra of single KPb_2Cl_5:0.5% Mn^{2+} crystal by monitoring the emission at 615 nm are shown in Fig. 5. It consists of two broad featureless bands centered at 615 and 716 nm and the former can be undoubtedly assigned to the $^4T_{1g}(^4G) \rightarrow {}^6A_{1g}(^6S)$ transition. Since there is no intermediate energy state between the ground state $^6A_{1g}(^6S)$ and excited state $^4T_{1g}(^4G)$, the broad emission band at longer wavelength should not be associated with the electronic transition of Mn^{2+}. To elucidate the origin of the later superposed on the former band, the emission spectra at different temperatures under the 355 nm excitation have been measured and compared, as shown in Fig. 6. The 10 K, 77 K,

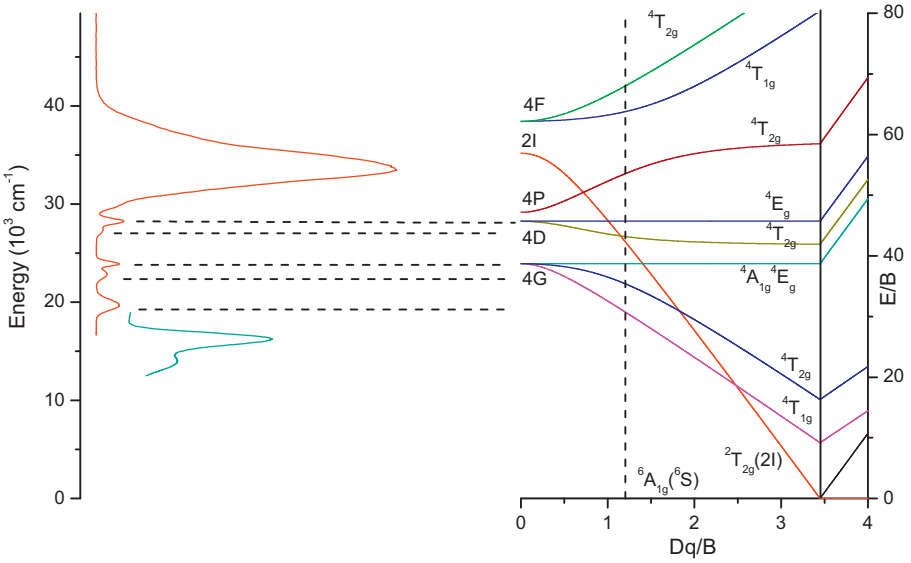

Fig. 5. The 77 K excitation and emission spectra of Mn^{2+} in KPb_2Cl_5 associated with the Tanabe–Sugano diagram. The vertical dash line indicates the appropriate value of Dq/B (1.2787) and the horizontal ones are used to correlate the peaks of the absorption of Mn^{2+} to the energy states in the Tanabe–Sugano diagram.

and room temperature emission spectra contain broad featureless bands centered at 601, 616, and 624 nm (marked by dash lines), respectively, which are associated with the $^4T_{1g}(^4G) \rightarrow {}^6A_{1g}(^6S)$ transition. Compared with the emission spectrum measured at 10 K, the maximum of this transition in the spectra measured at 77 K and room temperature shifts to high energy due to thermal population of upper state $^4T_{1g}(^4G)$. The emission spectra recorded at 77 and 10 K can be decomposed into two Gaussian peaks centered at 616 nm, 709 nm and 623 nm, 714 nm, respectively. The broad band in longer wavelength range vanishes when the temperature warms up to room temperature. Nikl et al. have observed a broad emission band in the spectral range from 500 to 800 nm excited by 300 nm at 4 K and tentatively attributed it to the radiation from Pb^{2+} ions with adjacent defects [38]. The increase of the temperature may lead to the luminescent quenching of these defects.

Turing to the 77 K excitation spectrum in Fig. 5 obtained by monitoring the 615 nm emission, it displays the characteristic absorption of divalent manganese compared with that of MnF_2 [39]. The orbital energy levels of five *d* orbital in an octahedral field can be characterized by the irreducible representations of the point group O_h. These five orbitals, which degenerate in the free ion, split into a triply degenerate set of $d\varepsilon$ orbital and a double degenerate set of $d\gamma$ orbital corresponding to the representations t_{2g} and e_g, respectively. Divalent manganese has a d^5 configuration and its ground state level is $^6A_{1g}(^6S)$. Note that $^4E_g(^4G)$, $^4A_{1g}(4G)$, $^4E_g(^4D)$, $^4A_{2g}(^4F)$ have the same orbital configuration as the ground state whereas $^4T_{1g}(^4G)$, $^4T_{2g}(^4G)$, $^4T_{2g}(^4D)$, $^4T_{1g}(^4P)$, $^4T_{1g}(^4F)$, and $^4T_{2g}(^4F)$ contain admixtures of the $d\varepsilon^4d\gamma^1$ and $d\varepsilon^2d\gamma^3$ configurations. Transitions between states of different orbital electronic configurations should be broad compared to those between states of the same electronic configuration [38–40], which is very useful in the assignment of the origin of each band. However, those considerations are only qualitative analysis and are not determinative on spectral assignment of Mn^{2+}. Tanabe and Sugano have tabulated the reduced matrix elements for d^5 in term of the Racah parameters *B* and *C* and the crystal field splitting parameters and the Tanabe–Sugano diagram is very useful in the spectral assignment of the transition metal ions [24,41]. The 77 K excitation spectrum of KPb_2Cl_5:0.5% Mn^{2+} can be interpreted with the aid of the Tanabe–Sugano diagram for octahedrally coordinated manganese. Francis and co-workers [42] pointed out that the A_{1g}, A_{2g}, and E_g states are not mixed by the octahedral crystal field and are therefore 10*Dq* independent. The sharp bands in the excitation spectrum in Fig. 4 centered at 354 and 418 nm are confidently attributed to the spin and parity forbidden transitions $^4E_g(^4D) \rightarrow {}^6A_{1g}(^6S)$ and $^4E_g(^4G) \rightarrow {}^6A_{1g}(^6S)$, respectively, which are *Dq* independent. By the above assignment, the Racah parameters *B* and *C* for the octahedrally coordinated Mn^{2+} can be calculate: $17B + 5C = E(^4E_g(^4D))$ and $10B + 5C = E(^4Eg(^4G))$. Thus $B = 618\ cm^{-1}$, $C = 3549\ cm^{-1}$, and $\gamma = C/B = 5.74$ are obtained.

Provided $\gamma = C/B = 5.74$ is known, it is possible to plot the Tanabe–Sugano diagram for Mn^{2+} in KPb_2Cl_5 by the use of the reduced matrix element tabulated in Ref. [24] and the derived diagram is shown in Fig. 5. Only quartet excited states, e.g. ^4G, ^4D, ^4P, and ^4F, are included except for $^2T_{2g}(^2I)$ since $^2T_{2g}(^2I)$ becomes the ground state when the value of *Dq*/*B* is larger than 3.447 whereas $^6A_{1g}(^6S)$ is the ground state when the value of *Dq*/*B* is smaller than this value. To obtain the crystal field splitting parameter 10*Dq*, the full matrices tabulated by Tanabe and Sugano in Ref. [24] were diagonalized over a range of *Dq*/*B* vales from 1 to 4 and the best fitting made to the features in the 77 K excitation spectrum in Fig. 5. By this fitting, the value of $Dq/B = 1.2787$ of Mn^{2+} in KPb_2Cl_5 was derived and thus $10Dq = 7902\ cm^{-1}$. It is evident that most of the absorption bands in the 77 K excitation spectrum in Fig. 5 can roughly be associated with the upper quartet states, as marked by horizontal dashed lines. The results calculated by the crystal field calculations are assembled in Table 1, in which the obtained parameters, Racah parameters, *B* and *C*, and the crystal splitting parameter $\Delta E = 10Dq$ are compared with those of a variety of hosts.

Table 1
Comparison of Racah and crystal field splitting 10*Dq* parameters of eight-coordinated Mn^{2+} in a variety of hosts.

Host	$B\ (cm^{-1})$	$C\ (cm^{-1})$	$10Dq\ (cm^{-1})$	References
Free ion	786	3790	–	[42]
Fluoride				
$RbMnF_3$	840	3080	7800	[44]
Oxide				
MnO	786	3210	9790	[46]
$Mn(H_2O)_6^{2+}$	671	3710	8480	[47]
Chloride				
KPb_2Cl_5	618	3549	7902	This work
$MnCl_2{\cdot}2H_2O$	630	3600	8000	[48]
Bromide				
$CdBr_2$	606	3499	–	[49]
Sulfide				
MnS	583	3125	7300	[50]
$MnPS_3$	494	3349	8750	[42]

It should be pointed out that the crystal field parameters such as 10*Dq* and *B* depend on (i) the nature of ligands; (ii) the coordination number; (iii) the metal–ligand distance; (iv) the type of host lattice where the complex is inserted, which has been previously addressed by Jørgensen [43], Moreno and co-workers [44,45]. It is meaningless to compare these parameters of Mn^{2+} complexes with a sixfold coordination with those with a fourfold or eight-fould coordination. The data summarized in Table 1 indicate that the value of the Racah and crystal field splitting parameters of Mn^{2+} in KPb_2Cl_5 are fairly typical of those found in a variety of other manganese compounds in which the Mn^{2+} ions are eight coordinated. The values of *B* are gradually reduced from free manganese ion to manganese in crystal hosts, which can be attributed to the increase of the degree of covalent bonding between manganese ion and the ligands [45].

3.3. Lifetime decay curves

The broad emission band centered in the range from 520 to 700 nm is associated with the parity and spin forbidden transition $^4T_{1g}(^4G) \rightarrow {}^6A_{1g}(^6S)$ and therefore the lifetime of this transition is expected to be much longer (in millisecond range) than those of parity allowed transitions of other transition metals. The lifetime decay curves measured at room temperature are mono-exponential and the lifetime is estimated to be 0.40 ± 0.02 ms (Fig. 7).

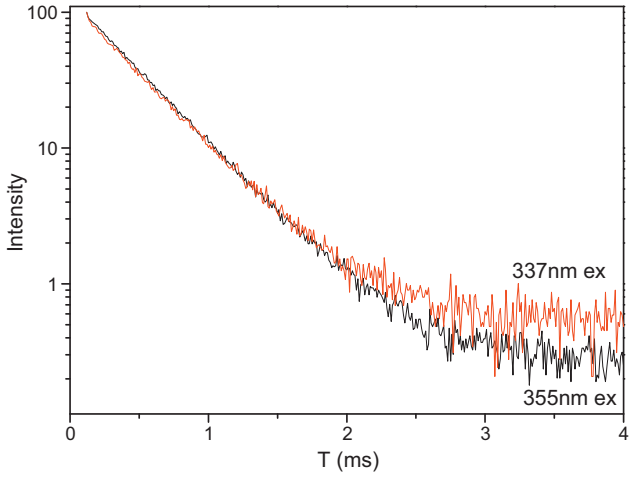

Fig. 7. Room temperature lifetime decay curve of KPb_2Cl_5:0.5% Mn^{2+} by monitoring the 601 nm emission. The excitation wavelengths are marked on the spectra.

4. Conclusions

By careful choosing the preparation conditions, transparent KPb_2Cl_5 containing 0.5% Mn^{2+} with good optical quality was successfully obtained. The photoluminescence excitation and emission spectra of Mn^{2+} in KPb_2Cl_5 have been measured and interpreted with the use of the Tanabe–Sugano diagram by assuming Mn–Cl groups form the octahedron with some approximation. The derived crystal field splitting parameter $10Dq$, Racah parameters B and C of Mn^{2+} in KPb_2Cl_5 fall into the range of those of other chloride hosts and have been compared with a variety of host matrices. Good agreement was obtained between the experimental spectroscopic data and the data calculated by use of the above crystal field parameters. Although the red emission presented at low temperature only was tentatively assigned to the emission of Pb^{2+} defects, this emission is rather complicated and further work is currently in progress to elucidate its origin.

Acknowledgements

This research is supported by the Project of the National Nature Science Foundation of China (Grant Nos. 11004177 and 51072190), Program for New Century Excellent Talents in University (Grant No. NCET-07-0786), and the Nature Science Foundation of Zhejiang Province (Grant No. Z4100030, Y1110139 and Y4110416).

References

[1] A.N. Vtyurin, L.I. Isaenko, S.N. Krylova, A. Yelisseyev, A.P. Shebanin, P.P. Turchin, N.G. Zamkova, V.I. Zinenko, Phys. Stat. Sol. C 1 (2004) 3142.
[2] A. Ferrier, M. Velázquez, J.-L. Doualan, R. Moncorgé, J. Opt. Soc. Am. B 24 (2007) 2526.
[3] R. Balda, J. Fernández, A. Mendioroz, M. Voda, M. Al-Saleh, Phys. Rev. B 68 (2003) 165101.
[4] C. Cascales, J. Fernández, R. Balda, Opt. Express 13 (2003) 2141.
[5] R. Balda, A.J. Garcia-Adeva, M. Voda, J. Fernández, Phys. Rev. B 69 (2004) 205203.
[6] J. Fernández, A.J. Garcia-Adeva, R. Balda, Phys. Rev. Lett. 97 (2006) 033001.
[7] G.H. Jia, P.A. Tanner, C.Y. Tu, J.F. Li, M.-Y. Lin, B.-M. Cheng, Appl. Phys. Lett. 92 (2008) 101115.
[8] N.W. Jenkins, S.R. Bowman, S. O'Connor, S.K. Searles, J. Ganem, Opt. Mater. 22 (2003) 311.
[9] M. Velázquez, J.-F. Marucco, P. Mounaix, O. Pérez, A. Ferrier, R. Moncorgé, Cryst. Growth Des. 9 (2009) 1949.
[10] N.J. Condon, S.R. Bowman, S.P. O'Connor, R.S. Quimby, C.E. Mungan, Opt. Express 17 (2009) 5466.
[11] A.A. Merkulov, L.I. Isaenko, V.M. Pashkov, V.G. Mazur, A.V. Virovets, D.Yu. Naumov, J. Struct. Chem. 46 (2005) 103.
[12] R.D. Shannon, Acta Cryst. A 32 (1976) 751.
[13] C. Neamtu, Al. Darabont, J. Optoelectron. Adv. Mater. 10 (2008) 2360.
[14] J.B. Gruber, R.M. Yow, A.S. Nijar, C.C. Russell III, D.K. Sardar, B. Zandi, A. Burger, U.N. Roy, J. Appl. Phys. 100 (2006) 043108.
[15] R. Balda, M. Voda, M. Al-Saleh, J. Fernández, J. Lumin. 97 (2002) 190.
[16] E. Brown, U. Hömmerich, A.G. Bluiett, S.B. Trivedi, J.M. Zavada, J. Appl. Phys. 101 (2007) 113103.
[17] A.J. Garcia-Adeva, R. Balda, J. Fernández, Opt. Mater. 31 (2009) 1075.
[18] M.C. Nostrand, R.H. Page, S.A. Payne, L.I. Isaenko, A.P. Yelissevev, J. Opt. Soc. Am. B 18 (2001) 264.
[19] A.G. Bluiett, E. Pinkney, E.E. Brown, U. Hömmerich, P. Amedzake, S.B. Trivedi, J.M. Zavada, Mater. Sci. Eng. B 146 (2008) 110.
[20] N.J. Condon, S. O'Connor, S.R. Bowman, J. Cryst. Growth 291 (2006) 472.
[21] U.N. Roy, Y. Cui, M. Guo, M. Groza, A. Burger, G.J. Wagner, T.J. Carrig, S.A. Payne, J. Cryst. Growth 258 (2003) 331.
[22] M. Velázquez, A. Ferrier, J.-P. Chaminade, B. Menaert, R. Moncorgé, J. Cryst. Growth 286 (2006) 324.
[23] Y. Wang, J.F. Li, C.Y. Tu, Z.Y. You, Z.J. Zhu, B.C. Wu, Cryst. Res. Technol. 42 (2007) 1063.
[24] Y. Tanabe, S. Sugano, J. Phys. Soc. Jpn. 9 (1954) 753.
[25] J.-S. An, J.H. Noh, I.-S. Cho, H.-S. Roh, J.-Y. Kim, H.-S. Han, K.-S. Hong, J. Phys. Chem. C 114 (2010) 10330.
[26] T.-S. Chan, R.-S. Liu, I. Baginskiy, Chem. Mater. 20 (2008) 1215.
[27] Y.-C. Chang, C.-H. Liang, S.-A. Yan, Y.-S. Chang, J. Phys. Chem. C 114 (2010) 3645.
[28] C.-J. Duan, A.C.A. Delsing, H.T. Hintzen, Chem. Mater. 21 (2009) 1010.
[29] H.A. Höppe, M. Daub, M.C. Bröhmer, Chem. Mater. 19 (2007) 6358.
[30] K.Y. Jung, H.W. Lee, Y.C. Kang, S.B. Park, Y.S. Yang, Chem. Mater. 17 (2005) 2729.
[31] K.H. Kwon, W.B. Im, H.S. Jang, H.S. Yoo, D.Y. Jeon, Inorg. Chem. 48 (2009) 11525.
[32] Z.-Y. Mao, D.-J. Wang, Inorg. Chem. 49 (2010) 4922.
[33] A.K. Sharma, K.H. Son, B.Y. Han, K.-S. Sohn, Adv. Funct. Mater. 20 (2010) 1750.
[34] A.K. Sharma, C. Kulshreshtha, K.S. Sohn, Adv. Funct. Mater. 19 (2009) 1705.
[35] D.T. Palumbo, J.J. Brow Jr., J. Electrochem. Soc. 117 (1970) 1184.
[36] D.T. Palumbo, J.J. Brow Jr., J. Electrochem. Soc. 118 (1971) 1159.
[37] A. Trueba, P. Garcia-Fernandez, J.M. García-Lastra, J.A. Aramburu, M.T. Barriuso, M. Moreno, J. Phys. Chem. A 115 (2011) 1423.
[38] M. Nikl, K. Nitsch, I. Velicka, J. Hybler, K. Polak, T. Fabian, Phys. Stat. Sol. B 168 (1991) K37.
[39] J.W. Stout, J. Chem. Phys. 31 (1959) 709.
[40] G. Blasse, B.C. Grabmaier, Luminescent Materials, Springer-Verlag, Berlin, 1994.
[41] S. Sugano, Y. Tanabe, H. Kamimura, Multiplets of Transition-Metal Ion in Crystal, Academic Press, New York, London, 1970.
[42] J. Boerio-Goates, E. Lifshitz, A.H. Francis, Inorg. Chem. 20 (1981) 3019.
[43] C.K. Jørgensen, Modern aspects of ligand field theory, North Holland Pub. Co., Amsterdam, 1971.
[44] M.T. Barriuso, M. Moreno, Chem. Phys. Lett. 112 (1984) 165.
[45] A. Trueba, J.M. García-Lastra, M.T. Barriuso, J.A. Aramburu, M. Moreno, Phys. Rev. B 78 (2008) 075108.
[46] G.W. Pratt Jr., R. Coelho, Phys. Rev. 116 (1959) 281.
[47] L.J. Heidt, G.F. Koster, A.M. Johnson, J. Am. Chem. Soc. 80 (1959) 6471.
[48] K.E. Lawson, J. Chem. Phys. 44 (1966) 4159.
[49] M.R. Panasyuk, V.E. Goncharuk, I.M. Kravchuk, S.S. Novosad, I.S. Novosad, Inorg. Mater. 41 (2005) 182.
[50] R.A. Ford, E. Kauer, A. Rabenau, D.A. Brown, Ber. Bunsenges. Phys. Chem. 67 (1963) 460.